

# Correlated High-Pressure Phase Sequence of VO<sub>2</sub> under Strong Compression

HPSTAR  
553-2018

Sheng-Yi Xie,<sup>†,‡,§</sup> Luhong Wang,<sup>§</sup> Fuyang Liu,<sup>†</sup> Xian-Bin Li,<sup>||</sup> Ligang Bai,<sup>⊥</sup> Vitali B. Prakapenka,<sup>#</sup> Zhonghou Cai,<sup>∇</sup> Ho-kwang Mao,<sup>†,○</sup> Shengbai Zhang,<sup>||,◆,¶</sup> and Haozhe Liu<sup>\*,†,§</sup>

<sup>†</sup>Center for High Pressure Science and Technology Advanced Research, Changchun and Beijing 130012, China

<sup>‡</sup>School of Physics and Electronics, Hunan University, Changsha 410082, China

<sup>§</sup>Harbin Institute of Technology, Harbin 150080, China

<sup>||</sup>State Key Laboratory on Integrated Optoelectronics, College of Electronic Science and Engineering, Jilin University, Changchun 130012, China

<sup>⊥</sup>Institute of High Energy Physics, Chinese Academy of Sciences, Beijing 100049, China

<sup>#</sup>Center for Advanced Radiation Sources, University of Chicago, Chicago, Illinois 60637, United States

<sup>∇</sup>Advanced Photon Source, Argonne National Laboratory, Argonne, Illinois 60439, United States

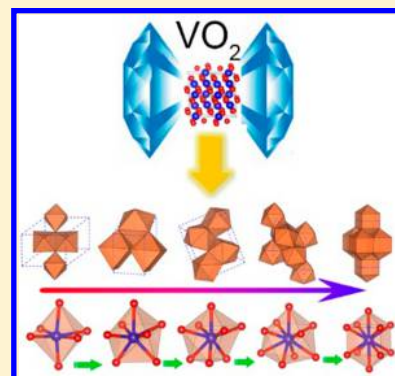
<sup>○</sup>Geophysical Laboratory, Carnegie Institution for Science, Washington, D.C. 20015, United States

<sup>◆</sup>Department of Physics, Applied Physics, and Astronomy, Rensselaer Polytechnic Institute, Troy, New York 12180, United States

<sup>¶</sup>Beijing Computational Science Research Center, Beijing 100094, China

## Supporting Information

**ABSTRACT:** Understanding how the structures of a crystal behave under compression is a fundamental issue both for condensed matter physics and for geoscience. Traditional description of a crystal as the stacking of a unit cell with special symmetry has gained much success on the analysis of physical properties. Unfortunately, it is hard to reveal the relationship between the compressed phases. Taking the family of metal dioxides (MO<sub>2</sub>) as an example, the structural evolution, subject to fixed chemical formula and highly confined space, often appears as a set of random and uncorrelated events. Here we provide an alternative way to treat the crystal as the stacking of the coordination polyhedron and then discover a unified structure transition pattern, in our case VO<sub>2</sub>. X-ray diffraction (XRD) experiments and first-principles calculations show that the coordination increase happens only at one apex of the V-centered octahedron in an orderly fashion, leaving the base plane and the other apex topologically intact. The polyhedron evolves toward increasing their sharing, indicating a general rule for the chemical bonds of MO<sub>2</sub> to give away the ionicity in exchange for covalency under pressure.



Like a temperature or external field, pressure can profoundly alter the physical behavior of a substance. For instance, applying high pressure can cause a phase transition, which is often accompanied by a structural change with atomic rearrangement due to the compressed volume and increased coordination number (CN), and subsequently a change in the materials' physical properties. Such a change can be vital for material science and geological and mineral physics. A lot has been done in the past to characterize such changes, as in principle they can be measured by various experiments such as XRD and Raman, or infrared, techniques. How the applied pressure affects the bonding network, whose change serves as the prerequisite for the structural change and phase transition, is more important but much less known. Taking ambient metal dioxides (MO<sub>2</sub>) as an example, where M is a metal cation, the typical structure comprises M-centered octahedrons that may be viewed as having a square basal plane, consisting of four

corner oxygen atoms and the M atom, capped by two oxygen apices. A series of TiO<sub>2</sub> phase transitions were confirmed through the distortion of the octahedrons at CN = 6 and the formation of postoctahedrons at CN > 6.<sup>1–4</sup> A structural transformation of VO<sub>2</sub> was also found under pressure and accompanied by an insulator-to-metal transition.<sup>5</sup> So far, little is known about the relationship between these compressed phases, except for the change in coordination number.

The situation may originate from the understanding of a crystal. Traditionally, a crystal is considered as the stacking of a unit cell with special symmetry, which is usually characterized by a space group. This definition of a crystal has gained great

Received: March 13, 2018

Accepted: April 18, 2018

Published: April 18, 2018

success for analyzing some physical properties centered on symmetry, such as band structure, phonon vibration, or optical transition. Yet this definition of crystal limits the understanding for the high-pressure phase transformations, which is based on the change of local bonding and coordination, instead of symmetry, as the first-hand effect of compression.

In this paper, using  $\text{VO}_2$  as an example, we suggest an alternative way to describe the crystal as the stacking of the coordination polyhedra under strong compression. Following this description, we illustrate how the crystal structure evolves with pressure from CN = 6 at ambient conditions to CN = 10 (theory) and 9 (experiment; pressure  $\leq 214$  GPa). The increase in CN is realized by the formation of postoctahedrons (CN > 6), which can be characterized by a sequential oxygen insertion from 1 to 3 at one of the two apexes of the octahedron, forming a second basal plane. Conversely, the other apex and the original basal plane are topologically unchanged. To obtain CN = 10, the last inserted oxygen caps the second basal plane to form a bicapped cube. Accordingly, the oxygen sharing pattern also changes from corner to edge, and eventually to a mix between the edge and face to maintain the  $\text{VO}_2$  formula. Our literature analysis suggests that a similar transition also applies to other  $\text{MO}_2$ s' such as  $\text{TiO}_2$  and  $\text{SiO}_2$ . Thus, our new description of a crystal provides a general way to clarify the relationship between the structures driven by compression.

At ambient pressure,  $\text{VO}_2$  exhibits a rutile structure with the vanadium located in the center of the oxygen octahedron when the temperature exceeds 340 K. It will transform to a monoclinic phase (M1, space group of  $P2_1/c$ ) by distortion of the octahedron when cooled to room temperature, but whether this transition is Peierls- or Mott-type dominated is still debatable.<sup>6–8</sup> Previous experimental work suggested the monoclinic phase of  $\text{VO}_2$  is nonmagnetic,<sup>9</sup> but both LDA and GGA calculations indicate a ferromagnetic ground state.<sup>10</sup> To align with the experiment, we performed DFT calculations without spin polarization. Due to a relatively strong electron correlation effect in 3d transition metal elements, the inclusion of on-site Coulomb repulsion  $U$  is often necessary. Here, we used  $U = 4.2$  eV and on-site exchange  $J = 0.8$  eV to treat the d electrons of vanadium.<sup>7</sup> Figure 1 gives the static enthalpy difference of the predicted stable phases related to the  $P\bar{6}2m$  phase as a function of pressure. Monoclinic  $P2_1/c$   $\text{VO}_2$ , with 6-fold coordination of vanadium (simply identified as CN6), will

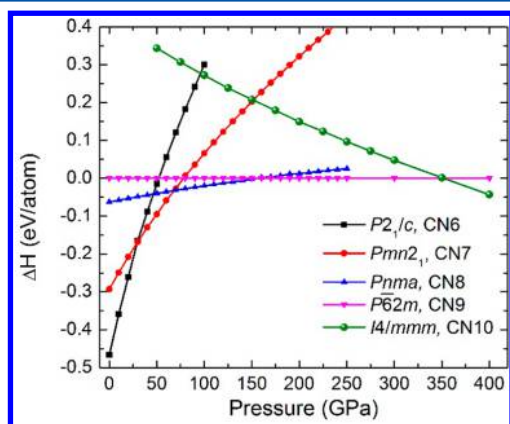


**Figure 1.** Relative static enthalpies of the compressed  $\text{VO}_2$  structures. The values are calculated by the PBE+U functional and plotted with the enthalpy of the  $P\bar{6}2m$  structure (CN = 9, the horizontal pink line) as a reference.

first transform to a 7-fold orthorhombic phase (space group of  $Pmn2_1$ , CN7), then to an 8-fold ( $Pnma$ , CN8), a 9-fold ( $P\bar{6}2m$ , CN9), and finally to a 10-fold coordination phase ( $I4/mmm$ , CN10). Interestingly, the CN8, CN9, and CN10 structures have been experimentally observed or theoretically predicted in other dioxides such as  $\text{TiO}_2$ <sup>2,4,11</sup> and  $\text{SiO}_2$ ,<sup>4,12</sup> yet CN7 is a new phase that has not been reported in  $\text{MO}_2$ . In previous work, this phase was responsible for the pressure-induced metalization and indexed as phase X,<sup>5</sup> yet the crystal structure of X phase is still debatable at present. Our work based on first-principles structure search and XRD method suggest the X phase should be orthorhombic  $Pmn2_1$  phase; see Figure S1 in the Supporting Information. Another candidate of the X phase is the monoclinic baddeleyite structure proposed by first-principles total energy calculations and Raman spectrum techniques,<sup>13</sup> or the monoclinic  $P1n1$  phase according to spin-polarized *ab initio* structure search and Raman scattering method.<sup>14</sup> Till present, it is still hard to determine the exact structure of X phase due to the limited precision to describe strongly correlated system by first-principles calculation and thus further high-pressure single-crystal diffraction experiment is needed in future.

Although  $\text{MO}_2$  high-pressure phases can be generally characterized by experiments or theoretical predictions, the relationship between them is rarely understood. In this work, we discovered that  $\text{VO}_2$  structures in a phase sequence from CN6 to CN10 exhibit a simple transition pattern. Instead of considering the possible transformations of the space group, we focused on the evolution of their coordination polyhedra. In the ambient CN6 phase, the characterized building block is a vanadium-centered octahedron, which connects with eight other neighboring octahedrons through corner sharing and two through edge sharing, as shown in Figure 2 and Table 1. Under compression, an oxygen atom previously belonging to other octahedrons is compelled to insert itself into the bottom apex of the octahedron. After completion, the octahedrons evolve into the so-called one-capped trigonal prism, and thus, CN6 transforms into the CN7 phase. The same transition pattern is also applied to achieve the CN8 and CN9 phases, with the polyhedra transforming to a dodecahedron<sup>15</sup> and tricapped trigonal prism.<sup>16</sup> Further to realizing the CN10 phase, the fourth inserted oxygen caps the rotated bottom basal plane of the tricapped trigonal prism in CN9, to form a bicapped cube.<sup>17</sup> A similar transition pattern also occurs in other  $\text{MO}_2$ s, such as  $\text{TiO}_2$ ,  $\text{ZrO}_2$ , or  $\text{SiO}_2$ . Ambient  $\text{TiO}_2$  has a rutile structure with CN = 6, which first transforms to a CN = 7 baddeleyite type structure, then to cotunnite and  $\text{Fe}_2\text{P}$ -type structures (both with CN = 9) under pressure, and finally to  $I4/mmm$  structure with CN = 10 according to first-principles prediction.<sup>4</sup>  $\text{ZrO}_2$ , starting with a baddeleyite structure with CN = 7 at ambient pressure, first transforms to an orthorhombic  $Pbca$  structure with the same CN and then to the CN = 9 cotunnite<sup>18</sup> and  $\text{Fe}_2\text{P}$ -type structure.<sup>19</sup> Different from  $\text{VO}_2$ , CN = 6 rutile  $\text{SiO}_2$  (stishovite) first transformed to a cubic pyrite ( $P\bar{a}3$ ) structure with six short and two other long coordination,<sup>20</sup> namely, CN = 6 + 2. Still no corresponding CN = 7 phase has been experimentally observed in  $\text{SiO}_2$ , and further larger CN phases (cotunnite- and  $\text{Fe}_2\text{P}$ -type with CN = 9 and  $I4/mmm$  with CN = 10) were predicted through first-principles calculations. Notably, cubic  $\text{TiO}_2$  was once synthesized at about 48 GPa and 2000 K by laser-heating in a diamond-anvil cell (DAC), yet the temperature effect is considered to be essential in the formation of the cubic phase.<sup>21</sup> Moreover, it is not possible to determine

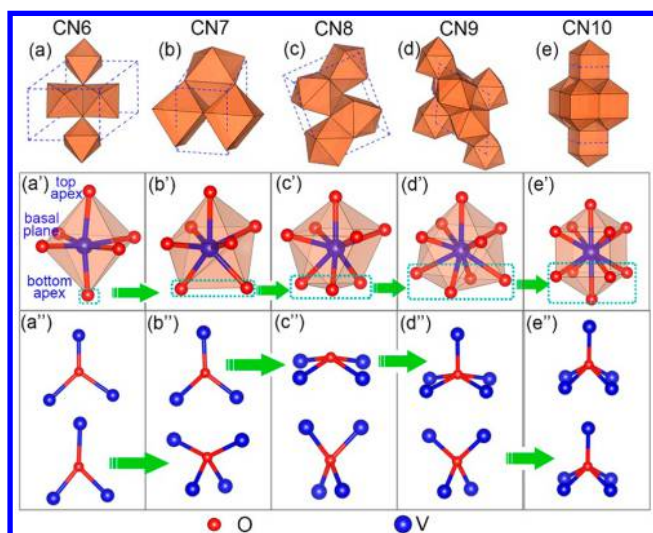


**Figure 2.** Crystal structures and related V-centered coordination polyhedra as the building blocks of VO<sub>2</sub>. (a)–(e) show the crystal structures and the stacking of the polyhedra in the CN6 to CN10 structures. Blue lines in (a)–(e) display the related unit cells of these structures. (a')–(e') illustrate the shape of the typical polyhedron in related structures, and (a'')–(e'') display the corresponding oxygen coordination motifs. The octahedron in CN6 can be divided into three parts: top and bottom apexes and basal plane in (a'). The dotted lines in (a')–(e') indicate that the coordination increase takes place only at the bottom apex of the octahedron. Green arrows indicate that the evolution of the polyhedron is accompanied by a change of the oxygen coordination. Vanadium and oxygen atoms are characterized by the big blue and small red balls, respectively.

**Table 1.** VO<sub>2</sub> Structures, Related Polyhedra, and Their Stacking Way

phases	polyhedra	corner sharing	edge sharing	triangular face sharing	quadrangular face sharing
CN6	octahedron	8	2	0	0
CN7	one-capped trigonal prism	5	6	0	0
CN8	dodecahedron	5	2	4	0
CN9	tricapped trigonal prism	0	3	5	0
CN10	bicapped cube	0	8	0	4

the exact symmetry (CN = 6 + 2 pyrite- or CN = 8 fluorite-type structure) of the cubic phase by the experimental data.<sup>21</sup> Although pyrite-type SiO<sub>2</sub> was well documented, a previous experimental study suggested that it is not likely to transform into the fluorite- but, instead, into the cotunnite-type structure,<sup>22</sup> as the theoretical study predicted.<sup>23</sup> Thus, TiO<sub>2</sub>, ZrO<sub>2</sub>, and SiO<sub>2</sub> have transition patterns similar to that of VO<sub>2</sub> where their polyhedra evolve in such a way that the inserting oxygen always occurs at the bottom. However, some compounds, such as RuO<sub>2</sub>, have another transition pattern. RuO<sub>2</sub> has a proven transformation from an orthorhombic CaCl<sub>2</sub>-type phase (CN = 6) to a CN = 6 + 2 pyrite structure<sup>24</sup> and finally to a cubic fluorite-type phase (CN = 8).<sup>25</sup> The polyhedral transition, in contrast to inserting oxygen always on one apex, adopts a symmetrical oxygen insertion on both the top and bottom apexes of the octahedron, as shown in Figure S2 in the Supporting Information.

The sharing mechanism among the VO<sub>2</sub> polyhedra also changes with the CN, from corner- and edge-sharing in CN6, to increasing edge sharing in CN7 and to face sharing in CN8

to CN10, Table 1. The Pauling third rule states that the cation coordination polyhedron of an ionic crystal would be most stable through corner sharing, less stable through edge sharing, and least stable through face sharing.<sup>26,27</sup> Thus, the emergence of edge sharing in VO<sub>2</sub> or TiO<sub>2</sub> signals a change of the metal–oxygen bond character to make the structure stable. It is expected that the covalent character of the metal–oxygen bond should increase and the ionic character should drop with greater shared polyhedral linking under strong compression. A Bader charge study supports the assumption that all the structures of CN6 to CN10 decrease the ionicity with pressure.

Moreover, the sequential structures have a tendency to drop the charge transfer for the metal–oxygen bond, as shown in Figure 3a. The Madelung energy calculation in Figure 3b,

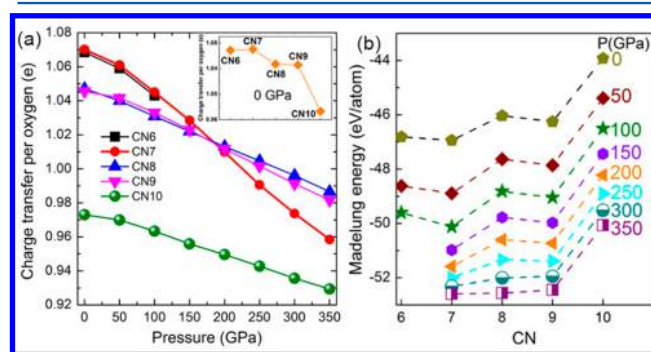


**Figure 3.** Bonding information on the compressed VO<sub>2</sub> structures. (a) Charge transfer to oxygen evaluated from Bader charge in the VO<sub>2</sub> structures with pressure. Inset specifically shows their charge transfer at 0 GPa. (b) Calculated Madelung energy variation with CN under chosen pressures.

assuming a fixed charge transfer of  $-2e$  per oxygen, also supports that increasing the CN by applying pressure tends to increase the Madelung energy. Thus, the effect of the increased CN is to reduce the ionic character of VO<sub>2</sub>. In short, the cation CN in MO<sub>2</sub> that increases with pressure and a fixed formula is realized through increased sharing with its neighboring coordination polyhedra, and meanwhile increasing the covalent character of the metal–oxygen bond stabilizes these edge-shared and even face-shared structures.

Figure 4a shows high-pressure XRD patterns varying with increasing pressure. The first experimental phase transition occurs at 29 GPa with the appearance of new Bragg diffraction peaks. The simulated CN7 phase agrees with the experimental data, as shown in Figure 4c, although the phase CN6 still coexists with the new phase until 79 GPa. The CN8 and CN9 phases also are verified by the XRD experiment, as shown in Figure 4d,e. The experimental transition pressures are 69 and 100 GPa, which are comparable with 70 and 150 GPa estimated from the PBE+U calculations. Besides, the CN7 phase is expected to be stable from 29 to 70 GPa, estimated by the PBE+U calculation in Figure 1, which also agrees with previous experimental study in which this phase was marked as unknown phase X.<sup>5</sup> Yet, the two phases of CN8 and CN9 have approachable energy in a wide pressure range from 70 to 250 GPa, as shown in Figure 1. This is also reflected from the XRD patterns in Figure 4d,e, in which the phases of CN8 always mix with phases of CN7 and CN9. Therefore, the CN8 phase might be metastable as proposed in previous theoretical calculations for same structure under strong compression in the case of SiO<sub>2</sub>.<sup>28</sup> In the present work, the CN10 phase was not observed

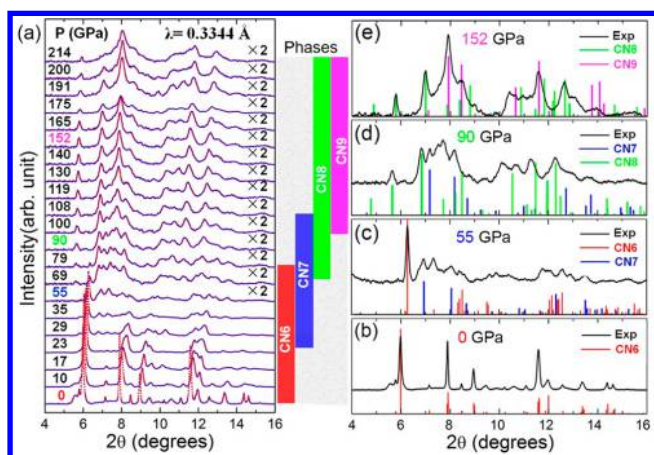


**Figure 4.** XRD patterns of the compressed  $\text{VO}_2$  sample. (a) Selected experimental XRD patterns of  $\text{VO}_2$  under various pressure conditions up to 214 GPa and the corresponding structures. (b)–(e) Contrast of the experimental and simulated XRD patterns based on the predicted high-pressure phases at (b) ambient pressure, (c) 55 GPa, (d) 90 GPa, and (e) 152 GPa.

in our experiment because its transition pressure is higher than our highest experimental pressure. The detailed lattice parameters, volume change, and phase alteration with pressure for CN6 to CN9 structures are shown in Figure S3 and Table S1 in the [Supporting Information](#).

Though Si, Ti, and V have different atomic orbitals, their dioxides display similar phases and coordination polyhedra. Therefore, cations are not an exclusive factor and oxygen properties have an important influence on these phases. As shown in [Figure 2](#), the evolution of cation polyhedra is, in fact, accompanied by an oxygen coordination change. As the hybridization of oxygen in 100% 3-fold, to 50%/50% 3- and 4-fold, to 100% 4-fold, to 50%/50% 4- and 5-fold, and finally to 100% 5-fold coordination forms, the CN cation gradually changes from 6 to 10. Furthermore, the shape of the oxygen coordination motifs, which is determined by oxygen orbital hybridization, significantly influence the cation polyhedra. For example, CN8  $\text{VO}_2$  has two unequal oxygen coordination motifs, with one considered approximately as  $\text{sp}^3$  hybridization and the other as  $p_x$ – $p_y$  hybridization, shown in [Figure 2c'](#), while for  $\text{RuO}_2$ , the structure of CN = 8<sup>25</sup> has two equal motifs with the same  $\text{sp}^3$  hybridization, as shown in [Figure S2](#) in the [Supporting Information](#). The difference of oxygen coordination between  $\text{VO}_2$  and  $\text{RuO}_2$  makes them exhibit different cation polyhedra, which further leads to different evolution patterns.

It is interesting to compare the phases of  $\text{VO}_2$  with other dioxides. The phase sequences of  $\text{SiO}_2$  induced by high pressure were theoretically predicted as CN6 structures (rutile,  $\text{CaCl}_2$ ,  $\alpha$ - $\text{PbO}_2$ ) CN(6 + 2) (pyrite), CN9 ( $Pnma$  and  $P\bar{6}2m$ ) structures,<sup>12,28</sup> but only the phases up to the pyrite structure in  $\text{SiO}_2$  have been observed experimentally until now.<sup>20</sup> The two CN9 phases of  $\text{SiO}_2$  were predicted to be stable until at least 650 GPa,<sup>28</sup> which remains challenging for current static DAC experiments. For  $\text{TiO}_2$ , the ambient rutile phase first transformed to  $\alpha$ - $\text{PbO}_2$  (still in CN = 6) and then to the baddeleyite phase, to an orthorhombic (CN = 7) phase, a  $Pnma$  (CN9) phase, and  $P\bar{6}2m$  (CN9) phase.<sup>2,11</sup> The  $P\bar{6}2m$  phase of  $\text{TiO}_2$  was obtained by laser heating at 210 GPa and 4000 K in a DAC experiment.<sup>11</sup> The related transforming conditions are summarized in [Table S2](#) in the [Supporting Information](#). It is noted that other  $\text{MO}_2$ s, such as  $\text{GeO}_2$  or  $\text{PbO}_2$ , have relatively

lower transition pressures in a structure similar to that for  $\text{SiO}_2$ .<sup>29</sup> However, due to the scope limitation of the present work, they are not included in detailed discussion here. In the present study, under cold compression, CN6  $\text{VO}_2$  transformed to a new CN7, then to the CN8 phase at 70 GPa and CN9 at 100 GPa, where the transition pressure is much lower than that in  $\text{TiO}_2$  and  $\text{SiO}_2$ . Thus,  $\text{VO}_2$  can serve as a typical material to study the ultrahigh phases of other dioxides. For example, a theoretical study predicted that the CN10 structure of  $\text{TiO}_2$  and  $\text{SiO}_2$  should exist at pressures around 647 GPa and 10 TPa, respectively,<sup>4</sup> yet the same type of structure in  $\text{VO}_2$  is expected to become stable at about 350 GPa in [Figure 1](#).

In conclusion, a systematic study of the high-pressure phase sequences of  $\text{VO}_2$  suggests a correlated structural change with a unified transition pattern, which is best described by a simple evolution of the polyhedra with a coordination number increase. Altering the sharing pattern of the oxygen atoms at the corners of the polyhedra allows for denser packing of the atoms in response to the applied pressure. Consequently, the crystal gives away its ionicity in exchange for covalency. As the observed evolution of the polyhedra and oxygen sharing pattern are both properties of the oxygen orbitals, our results suggest that these orbitals play an increasingly important role in determining the structure of  $\text{MO}_2$  under pressure. The evolution of M-centered polyhedra stated in this work provides a new way to describe the high-pressure behavior of  $\text{MO}_2$  crystals and the relation of high-pressure phases, which could be the key to understanding the chemistry of the bonding, crystal structure and phase sequence under strong compression.

## EXPERIMENTAL AND COMPUTATIONAL METHODS

The  $\text{VO}_2$  sample, provided by the Sigma-Aldrich Company, was loaded into a steel gasket chamber with a 40  $\mu\text{m}$  diameter size and then compressed in a DAC with a beveled culet size of 100–300  $\mu\text{m}$  at room temperature. A tiny Pt foil was loaded with the sample and used as a pressure marker.<sup>30</sup> The XRD experiment was carried out at GSECARS, beamline 13-ID-D of the Advanced Photon Source, Argonne National Laboratory. Synchrotron X-rays with a wavelength of 0.3344 Å were focused on the sample spot with a beam size of about 3  $\mu\text{m}$ . Global minimal structure searching was undertaken by CALYPSO code with the particle-swarm optimization algorithm,<sup>31,32</sup> which has been successfully used to predict high-pressure structures of transition metal compounds.<sup>33,34</sup> Total energy calculations based on a plane wave basis set were performed in VASP,<sup>35</sup> where the interaction of the ion cores and valence electrons is described by the projector augmented wave (PAW) method.<sup>36</sup> Perdew–Burke–Ernzerhof (PBE) of the generalized gradient approximation<sup>37</sup> with the Hubbard U method<sup>38</sup> was employed to describe the exchange and correlation interactions among the electrons. An energy cutoff of 900 eV and k-point sampling of  $2\pi \times 0.025 \text{ \AA}^{-1}$  were used to get the precise total energy.

## ASSOCIATED CONTENT

### Supporting Information

The Supporting Information is available free of charge on the ACS Publications website at DOI: 10.1021/acs.jpcllett.8b00771.

Experimental XRD patterns of  $\text{VO}_2$  with neon as a pressure-transmitting medium, polyhedra evolution of  $\text{RuO}_2$  high-pressure phases, lattice parameter and volume

change of VO<sub>2</sub> phases, Wyckoff positions of VO<sub>2</sub> phases, and phase transformed conditions for VO<sub>2</sub>, TiO<sub>2</sub>, and SiO<sub>2</sub> (PDF)

## AUTHOR INFORMATION

### Corresponding Author

\*H. Liu. E-mail: [haozhe.liu@hpstar.ac.cn](mailto:haozhe.liu@hpstar.ac.cn).

### ORCID

Sheng-Yi Xie: 0000-0002-9369-0914

### Author Contributions

S.-Y.X. and H.L. designed the project. S.-Y.X., L.W., F. L., and H.L. performed the XRD experiment. S.-Y.X., X.-B.L., and S.Z. took the crystal prediction and first-principles calculation. S.-Y.X., S.Z., and H.L. analyzed data and wrote the manuscript. All authors discussed the results and commented on the manuscript.

### Notes

The authors declare no competing financial interest.

## ACKNOWLEDGMENTS

This work was supported by National Science Associated Funding (U153042), Natural Science Foundation of China (11374075, 11374119, 11704111, 91423102, 91323301), Heilongjiang Province Science Fund for Distinguished Young Scholars (JC201005), Longjiang Scholar, the Fundamental Research Funds for the Central Universities (HIT. BRET1.2010002, HIT. IBRSEM.A.201403, HNU. 531107050916). S.Z. was supported by the U.S. Department of Energy (DoE) under Grant No. DE-SC0002623. The XRD experiment was performed at the Argonne National Laboratory and use of the Advanced Photon Source was supported by the U.S. DoE, Office of Science, Office of Basic Energy Sciences, under contract No. DE-AC02-06CH11357. GSECARS is supported by the National Science Foundation (NSF)-Earth Sciences (EAR-1128799) and DoE-GeoSciences (DE-FG02-94ER14466). Use of the COMPRES-GSECARS gas loading system was supported by COMPRES under NSF Cooperative Agreement EAR 11-57758. Part of the calculations were made on the High Performance Computing Center at Jilin University.

## REFERENCES

- (1) Dubrovinskaia, N. A.; Dubrovinsky, L. S.; Ahuja, R.; Prokopenko, V. B.; Dmitriev, V.; Weber, H. P.; Osorio-Guillen, J. M.; Johansson, B. Experimental and Theoretical Identification of a New High-Pressure TiO<sub>2</sub> Polymorph. *Phys. Rev. Lett.* **2001**, *87*, 275501.
- (2) Al-Khatatbeh, Y.; Lee, K. K. M.; Kiefer, B. High-Pressure Behavior of TiO<sub>2</sub> was Determined by Experiment and Theory. *Phys. Rev. B: Condens. Matter Mater. Phys.* **2009**, *79*, 134114.
- (3) Zhou, X.-F.; Dong, X.; Qian, G.-R.; Zhang, L.; Tian, Y.; Wang, H.-T. Unusual Compression Behavior of TiO<sub>2</sub> Polymorphs from First Principles. *Phys. Rev. B: Condens. Matter Mater. Phys.* **2010**, *82*, 060102.
- (4) Lyle, M. J.; Pickard, C. J.; Needs, R. J. Prediction of 10-Fold Coordinated TiO<sub>2</sub> and SiO<sub>2</sub> Structures at Multimegabar Pressures. *Proc. Natl. Acad. Sci. U. S. A.* **2015**, *112*, 6898–6901.
- (5) Bai, L.; Li, Q.; Corr, S. A.; Meng, Y.; Park, C.; Sinogeikin, S. V.; Ko, C.; Wu, J.; Shen, G. Pressure-Induced Phase Transitions and Metallization in VO<sub>2</sub>. *Phys. Rev. B: Condens. Matter Mater. Phys.* **2015**, *91*, 104110.
- (6) Wentzcovitch, R. M.; Schulz, W. W.; Allen, P. B. VO<sub>2</sub>: Peierls or Mott-Hubbard? A View from Band Theory. *Phys. Rev. Lett.* **1994**, *72*, 3389–3392.
- (7) Liebsch, A.; Ishida, H.; Bihlmayer, G. Coulomb Correlations and Orbital Polarization in the Metal-Insulator Transition of VO<sub>2</sub>. *Phys. Rev. B: Condens. Matter Mater. Phys.* **2005**, *71*, 085109.
- (8) Haverkort, M. W.; Hu, Z.; Tanaka, A.; Reichelt, W.; Streltsov, S. V.; Korotin, M. A.; Anisimov, V. I.; Hsieh, H. H.; Lin, H. J.; Chen, C. T.; Khomskii, D. I.; Tjeng, L. H. Orbital-Assisted Metal-Insulator Transition in VO<sub>2</sub>. *Phys. Rev. Lett.* **2005**, *95*, 196404.
- (9) Umeda, J. i.; Kusumoto, H.; Narita, K.; Yamada, E. Nuclear Magnetic Resonance in Polycrystalline VO<sub>2</sub>. *J. Chem. Phys.* **1965**, *42*, 1458–1459.
- (10) Yuan, X.; Zhang, Y.; Abtey, T. A.; Zhang, P.; Zhang, W. VO<sub>2</sub>: Orbital Competition, Magnetism, and Phase Stability. *Phys. Rev. B: Condens. Matter Mater. Phys.* **2012**, *86*, 235103.
- (11) Dekura, H.; Tsuchiya, T.; Kuwayama, Y.; Tsuchiya, J. Theoretical and Experimental Evidence for a New Post-Cotunnite Phase of Titanium Dioxide with Significant Optical Absorption. *Phys. Rev. Lett.* **2011**, *107*, 045701.
- (12) Tsuchiya, T.; Tsuchiya, J. Prediction of a Hexagonal SiO<sub>2</sub> Phase Affecting Stabilities of MgSiO<sub>3</sub> and CaSiO<sub>3</sub> at Multimegabar Pressures. *Proc. Natl. Acad. Sci. U. S. A.* **2011**, *108*, 1252–1255.
- (13) Chen, Y.; Zhang, S.; Ke, F.; Ko, C.; Lee, S.; Liu, K.; Chen, B.; Ager, J. W.; Jeanloz, R.; Eyert, V.; Wu, J. Pressure-Temperature Phase Diagram of Vanadium Dioxide. *Nano Lett.* **2017**, *17*, 2512–2516.
- (14) Balédent, V.; Cerqueira, T. T. F.; Sarmiento-Pérez, R.; Shukla, A.; Bellin, C.; Marsi, M.; Itié, J.-P.; Gatti, M.; Marques, M. A. L.; Botti, S.; Rueff, J.-P. High-pressure Phases of VO<sub>2</sub> from the Combination of Raman Scattering and *Ab Initio* Structural Search. *Phys. Rev. B: Condens. Matter Mater. Phys.* **2018**, *97*, 024107.
- (15) Porai-Koshits, M.; Aslanov, L. Some Aspects of the Stereochemistry of Eight-Coordinate Complexes. *J. Struct. Chem.* **1972**, *13*, 244–253.
- (16) Ruiz-Martinez, A.; Casanova, D.; Alvarez, S. Polyhedral Structures with an Odd Number of Vertices: Nine-Coordinate Metal Compounds. *Chem. - Eur. J.* **2008**, *14*, 1291–303.
- (17) Ruiz-Martinez, A.; Alvarez, S. Stereochemistry of Compounds with Coordination Number Ten. *Chem. - Eur. J.* **2009**, *15*, 7470–80.
- (18) Al-Khatatbeh, Y.; Lee, K. K. M.; Kiefer, B. Phase Relations and Hardness Trends of ZrO<sub>2</sub> Phases at High Pressure. *Phys. Rev. B: Condens. Matter Mater. Phys.* **2010**, *81*, 214102.
- (19) Nishio-Hamane, D.; Dekura, H.; Seto, Y.; Yagi, T. Theoretical and Experimental Evidence for the Post-Cotunnite Phase Transition in Zirconia at High Pressure. *Phys. Chem. Miner.* **2015**, *42*, 385–392.
- (20) Kuwayama, Y.; Hirose, K.; Sata, N.; Ohishi, Y. The Pyrite-Type High-Pressure Form of Silica. *Science* **2005**, *309*, 923–925.
- (21) Mattesini, M.; de Almeida, J. S.; Dubrovinsky, L.; Dubrovinskaia, N.; Johansson, B.; Ahuja, R. High-Pressure and High-Temperature Synthesis of the Cubic TiO<sub>2</sub> Polymorph. *Phys. Rev. B: Condens. Matter Mater. Phys.* **2004**, *70*, 212101.
- (22) Kuwayama, Y.; Hirose, K.; Sata, N.; Ohishi, Y. Pressure-Induced Structural Evolution of Pyrite-Type SiO<sub>2</sub>. *Phys. Chem. Miner.* **2011**, *38*, 591–597.
- (23) Oganov, A. R.; Gillan, M. J.; Price, G. D. Structural Stability of Silica at High Pressures and Temperatures. *Phys. Rev. B: Condens. Matter Mater. Phys.* **2005**, *71*, 064104.
- (24) Haines, J.; Leger, J. M.; Schulte, O. Pa-3 Modified Fluorite-Type Structures in Metal Dioxides at High Pressure. *Science* **1996**, *271*, 629–631.
- (25) Tse, J. S.; Klug, D. D.; Uehara, K.; Li, Z. Q.; Haines, J.; Leger, J. M. Elastic Properties of Potential Superhard Phases of RuO<sub>2</sub>. *Phys. Rev. B: Condens. Matter Mater. Phys.* **2000**, *61*, 10029–10034.
- (26) Pauling, L. *The Nature of the Chemical Bond*; Cornell University Press: Ithaca, NY, 1962.
- (27) Burdett, J. K.; McLarnan, T. J. An Orbital Explanation for Pauling's Third Rule. *J. Am. Chem. Soc.* **1982**, *104*, 5229–5230.
- (28) Wu, S.; Umamoto, K.; Ji, M.; Wang, C.-Z.; Ho, K.-M.; Wentzcovitch, R. M. Identification of Post-Pyrite Phase Transitions in SiO<sub>2</sub> by a Genetic Algorithm. *Phys. Rev. B: Condens. Matter Mater. Phys.* **2011**, *83*, 184102.
- (29) Prakapenka, V. B.; Dubrovinsky, L. S.; Shen, G.; Rivers, M. L.; Sutton, S. R.; Dmitriev, V.; Weber, H. P.; Le Bihan, T.  $\alpha$ -PbO<sub>2</sub>-Type High-Pressure Polymorph of GeO<sub>2</sub>. *Phys. Rev. B: Condens. Matter Mater. Phys.* **2003**, *67*, 132101.

(30) Holmes, N. C.; Moriarty, J. A.; Gathers, G. R.; Nellis, W. J. The Equation of State of Platinum to 660 GPa (6.6 Mbar). *J. Appl. Phys.* **1989**, *66*, 2962–2967.

(31) Wang, Y.; Lv, J.; Zhu, L.; Ma, Y. Crystal Structure Prediction via Particle-Swarm Optimization. *Phys. Rev. B: Condens. Matter Mater. Phys.* **2010**, *82*, 094116.

(32) Wang, Y. C.; Lv, J.; Zhu, L.; Ma, Y. M. CALYPSO: A Method for Crystal Structure Prediction. *Comput. Phys. Commun.* **2012**, *183*, 2063–2070.

(33) Li, Q.; Zhou, D.; Zheng, W.; Ma, Y.; Chen, C. Global Structural Optimization of Tungsten Borides. *Phys. Rev. Lett.* **2013**, *110*, 136403.

(34) Bai, L.; Li, Q.; Corr, S. A.; Pravica, M.; Chen, C.; Zhao, Y.; Sinogeikin, S. V.; Meng, Y.; Park, C.; Shen, G. Pressure-Induced Cation-Cation Bonding in  $V_2O_3$ . *Phys. Rev. B: Condens. Matter Mater. Phys.* **2015**, *92*, 134106.

(35) Kresse, G.; Furthmüller, J. Efficient Iterative Schemes for *Ab Initio* Total-Energy Calculations Using a Plane-Wave Basis Set. *Phys. Rev. B: Condens. Matter Mater. Phys.* **1996**, *54*, 11169–11186.

(36) Blöchl, P. E. Projector Augmented-Wave Method. *Phys. Rev. B: Condens. Matter Mater. Phys.* **1994**, *50*, 17953–17979.

(37) Perdew, J. P.; Burke, K.; Ernzerhof, M. Generalized Gradient Approximation Made Simple. *Phys. Rev. Lett.* **1996**, *77*, 3865–3868.

(38) Liechtenstein, A. I.; Anisimov, V. I.; Zaanen, J. Density-Functional Theory and Strong Interactions: Orbital Ordering in Mott-Hubbard Insulators. *Phys. Rev. B: Condens. Matter Mater. Phys.* **1995**, *52*, R5467–R5470.